Geophysical Research Letters

RESEARCH LETTER
10.1029/2025GL119928

Identifying Energy Balance Drivers of Greenland Ice Sheet Surface Melt Using Causal Discovery

Ziqi Yin[1], Aneesh C. Subramanian[1], Rajashree Datta[2], Adam R. Herrington[3], Danni Du[4], Sahara Ali[5], Omar Faruque[6], and Jianwu Wang[6]

[1]Department of Atmospheric and Oceanic Sciences, University of Colorado at Boulder, Boulder, CO, USA, [2]Department of Geoscience and Remote Sensing, Delft University of Technology, Delft, The Netherlands, [3]Climate and Global Dynamics Laboratory, NSF National Center for Atmospheric Research, Boulder, CO, USA, [4]Program in Atmospheric and Oceanic Sciences, Princeton University, Princeton, NJ, USA, [5]Anuradha and Vikas Sinha Department of Data Science, University of North Texas, Denton, TX, USA, [6]Department of Information Systems, University of Maryland Baltimore County, Baltimore, MD, USA

Abstract Greenland Ice Sheet (GrIS) mass loss has accelerated in recent decades, primarily due to enhanced surface melt. Identifying the causal dependencies of surface melt remains challenging with conventional correlations. Using the PCMCI$^+$ causal discovery algorithm applied to CESM2 large-ensemble simulations and evaluated against two high-resolution regional climate models, we identify significant contemporaneous positive links from melt to net shortwave radiation (reflecting melt–albedo feedback) and from sensible and latent heat fluxes to melt. These results highlight shortwave radiation and turbulent heating as dominant drivers of GrIS summer melt anomalies over the ablation zone at monthly timescales. Compared with correlations, PCMCI$^+$ isolates fewer but more physically interpretable dependencies. By the end of the century (SSP3-7.0), these links persist but the turbulent heat-related ones become undirected, indicating reduced statistical identifiability and possible stronger instantaneous surface–atmosphere coupling in a warmer climate.

Plain Language Summary The Greenland Ice Sheet is melting faster, contributing to global sea level rise. Most of this melt occurs on the ice sheet surface during summer, but it remains unclear which processes are mainly responsible and how they might change in a warming climate. Here, we apply a causal discovery method that identifies cause-and-effect relationships, not just correlations, between atmospheric energy fluxes and surface melting. Using climate model simulations, we find that net solar radiation, sensible and latent heat flux are the main drivers of summer surface melt anomalies over the ablation zone during the historical period. By the end of this century, these links persist, but the turbulent heat-related ones become harder to distinguish in direction, suggesting possible stronger coupling between the atmosphere and the ice sheet surface in a warmer climate.

Key Points:

- Causal discovery identifies shortwave and turbulent heat as main melt-anomaly drivers, yielding clearer causal networks than correlations
- Global and regional climate models show consistent causal links between surface energy fluxes and melt variability
- Global warming makes turbulent heat-melt links undirected, suggesting potential stronger surface and atmosphere coupling

Supporting Information:

Supporting Information may be found in the online version of this article.

Correspondence to:

Z. Yin,
ziqi.yin@colorado.edu

Citation:

Yin, Z., Subramanian, A. C., Datta, R., Herrington, A. R., Du, D., Ali, S., et al. (2026). Identifying energy balance drivers of Greenland ice sheet surface melt using causal discovery. *Geophysical Research Letters*, *53*, e2025GL119928. https://doi.org/10.1029/2025GL119928

Received 24 OCT 2025
Accepted 19 MAY 2026

1. Introduction

Greenland Ice Sheet (GrIS) surface melt has intensified significantly since the 1990s (Zheng et al., 2025). As a result, the overall GrIS integrated surface mass balance (SMB) shifted from a low-variability, accumulation-dominated regime to a high-variability, melt-dominated regime, primarily due to ablation area expansion and bare ice season lengthening (Box et al., 2022; Fyke et al., 2014). Consequently, runoff has become more variable from year to year (Slater et al., 2021). Alongside continued increases in melt magnitude, interannual melt variability is projected to further increase toward the end of the century (van den Broeke et al., 2023).

To explain surface melt variability, previous studies have used cross-correlation, regression, and composite analysis to relate melt to energy fluxes and atmospheric conditions. Along the K-transect in west Greenland, van den Broeke et al. (2011) found that interannual melt variability in the higher ablation zone is mostly explained by net shortwave radiation, whereas variability in the lower ablation zone is dominated by sensible heat flux. This pattern is attributed to the quasi-constant summer albedo in the lower ablation zone, which limits the melt-albedo feedback, and to the proximity of the snow-free tundra, which heats up considerably in summer. They also projected that, with future ice retreat, the surface energy balance (SEB) and associated melt climate, as presently observed at low elevations, will become representative for the entire marginal ice sheet. For subseasonal day-to-day melt variability, sensible heat flux and shortwave radiation are the dominant factors at automatic weather stations (AWS) throughout the ablation zone (Wang et al., 2021). Sensible and solar heating correlate with the

occurrence of strong dry katabatic winds, which primarily increase surface sensible heating by enhancing vertical mixing, thereby reducing temperature inversion (Mattingly et al., 2023). The concomitant low humidity and clear skies yield increased solar heating. At the ice sheet margins, synoptic systems such as barrier winds, during which high wind speed combined with high temperature and cloud cover enhance turbulent heat fluxes and limit longwave heat loss, can also largely explain interdiurnal melt variability (van den Broeke et al., 2023). During extreme melt episodes, turbulent and other nonradiative fluxes can temporarily dominate melt across large parts of the ablation zone (Fausto et al., 2016), highlighting that the relative importance of SEB components shifts with atmospheric regime.

Understanding what drives this enhanced melt variability requires not only identifying co-occurring factors but also distinguishing between cause and effect while accounting for confounding influences. Traditional correlation-based methods are limited in this regard, affected by strong autocorrelations (Runge et al., 2014), and can produce spurious links between related processes (Vannitsem et al., 2019), motivating the use of causal discovery. Causal discovery aims to identify dominant, independent drivers of melt variability, not just correlations or instantaneous energy inputs, establish directionality, and distinguish direct from indirect influences, generating more interpretable causal graphs. There has been a growing interest in applying causal inference to Earth sciences in recent years (Karmouche et al., 2023; Krich et al., 2020; Runge, Bathiany, et al., 2019; Samarasinghe et al., 2019), but the application to ice sheet processes remains limited (Kromer & Trusel, 2023).

In this study, we explore the potential of causal discovery to reconstruct the causal structure underlying GrIS surface melt and address two questions: (1) What is the relative importance of the atmospheric SEB components and processes in driving GrIS surface melt anomalies on monthly and daily timescales? (2) With global warming, will there be a regime shift in this causal structure? In Section 2, the data and causal discovery method are introduced. Section 3 evaluates the causal graphs for a historical period and then examines how these relationships may change in a warmer climate. Section 4 summarizes the findings and outlines the study's contributions and limitations.

2. Methods

2.1. Data

To ensure robust statistics, we use monthly output of the 50 CMIP6 members of the CESM2 Large Ensemble (LENS2; Danabasoglu, Lamarque, et al., 2020; Rodgers et al., 2021), including historical (1850–2014) and future SSP3-7.0 scenario simulations (2015–2100), at ∼1° horizontal resolution.

For comparison with CESM2, we use two high-resolution regional climate models (RCMs)–Regional Atmospheric Climate Model (RACMO2.3p2; Noël et al., 2018) and Modèle Atmosphérique Régional (MARv3.14; Haacker et al., 2024), which reproduce historical meteorological and SMB measurements across the GrIS with good agreement (Fettweis et al., 2017; Noël et al., 2018). Their horizontal resolutions in this study are 5.5 and 10 km, respectively. While our primary analysis focuses on monthly timescales, we also examine daily RCM output to understand potential short-term lagged interactions.

In addition to surface melt (*Melt*), the four atmospheric SEB variables were selected, including net shortwave radiation (SW_n), net longwave radiation (LW_n), sensible heat flux (*SH*), and latent heat flux (*LH*). We prioritize the SEB fluxes not to disregard other influencing factors (e.g., clouds, Greenland blocking) but to establish the most direct causal links to surface melt. Since excluded variables may confound the energy fluxes, we focus exclusively on links involving *Melt*. Each variable is spatially integrated (*Melt*) or averaged (SEB fluxes) over the mean ablation zone of the corresponding model (masks shown in Figure 1), where surface melt primarily occurs.

2.2. Causal Discovery Method

PCMCI (Peter Clark Momentary Conditional Independence) is a causal discovery framework developed by Runge, Nowack, et al. (2019) that consists of two stages: (a) PC1 condition selection to identify potential causal parents by eliminating irrelevant variables and (b) MCI test to validate causal relationships and determine causal directions. PCMCI is suitable for autocorrelated, high-dimensional time series with nonlinear dependencies. PCMCI$^+$ is an updated version that can also detect contemporaneous causal links (Runge, 2020). It has been successfully applied in climate science to investigate phenomena such as teleconnections (Du et al., 2024; Karmouche et al., 2023) and ice sheet-climate interactions (Kromer & Trusel, 2023).

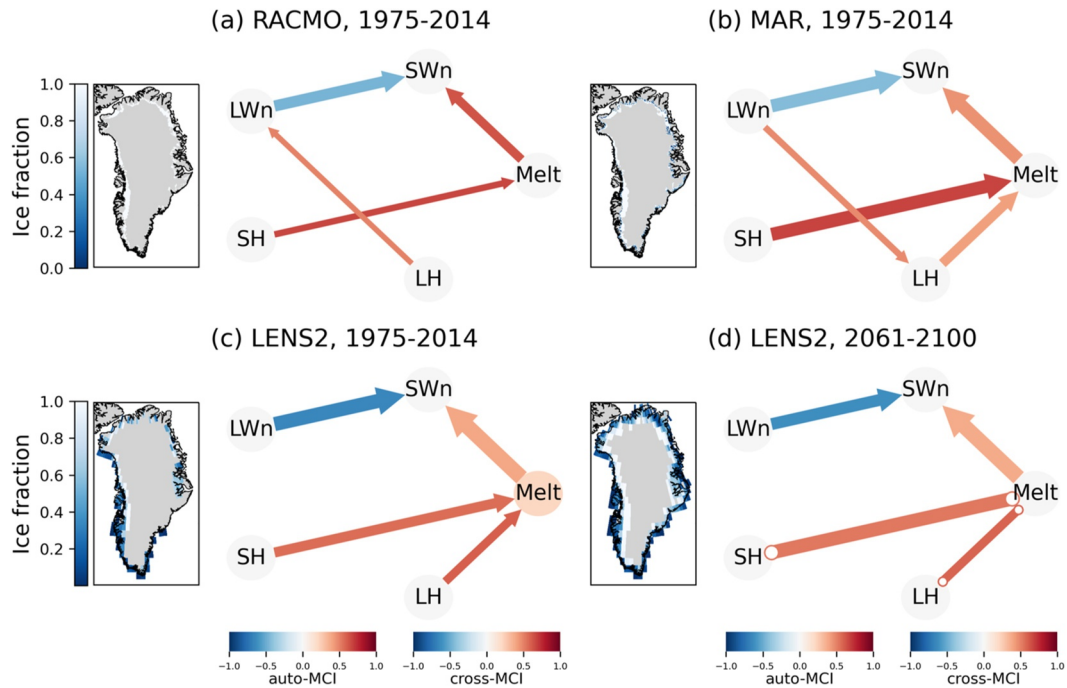

Figure 1. Causal graphs and corresponding ablation zone masks of the historical period 1975–2014 for RACMO (a), MAR (b), and CESM2 large ensemble (c); and of the end of the century 2061–2100 for CESM2 large ensemble (d). Straight arrows indicate contemporaneous directed links. Unoriented contemporaneous links denote that orientation rules cannot be applied ("∘ − ∘"). Node color indicates the maximum auto-MCI, defined as the partial correlation between a variable and its own past conditioned on relevant parents (gray indicates insignificant values). Link color indicates cross-MCI, defined as the partial correlation between two variables obtained from the conditional independence test. Link width increases monotonically with detection rate (0%–100%), defined as the percentage of bootstrap realizations in (a, b) and ensemble members in (c, d) in which the link type is detected.

PCMCI$^+$ relies on several assumptions, including the causal Markov condition, faithfulness, sufficiency, stationarity, acyclicity, and Gaussian noise distribution (Runge et al., 2023). For computational efficiency, interpretability, and stability (Krich et al., 2020; Runge, Nowack, et al., 2019), we restrict the analysis to linear dependencies by using a relatively short sample size (40 years) and use robust linear partial correlation (RobustParCorr) as the conditional independence test, which transforms variables to normally distributed marginals. Key parameters are set as follows: the minimum time delay $\tau_{\min} = 0$, and the maximum time delay $\tau_{\max} = 12$ months for monthly analyses and $\tau_{\max} = 15$ days for daily analyses. The significance level is set to $\alpha_{pc} = 0.05$ for all tests, chosen to yield a sufficient number of directed links while avoiding overly dense graphs.

The resulting graphs contain directed lagged (curved arrows, "$\overset{\tau}{\rightarrow}$") and contemporaneous links (straight arrows, "$\rightarrow$") and also unoriented contemporaneous links, indicating that the collider and orientation rules cannot be applied (Markov equivalence, circles on both ends, "∘ − ∘") or a conflicting adjacency when orientation rules disagree (crosses on both ends, "×−×"), for example, due to finite sample issues (see Text S2 in Supporting Information S1 for a conceptual explanation). If multiple lagged links occur, the one with the strongest cross-MCI (partial correlation value from the conditional independence test) value is displayed, along with its associated lag. Node color indicates the maximum auto-MCI (partial correlation between a variable and its own past, conditioned on relevant parents) value for each variable if significant, regardless of lags. An example of causal graphs is shown in Figure 1.

2.3. Data Preprocessing

Preprocessing consists of three steps: detrending, normalization, and seasonal masking. First, the time series are detrended with a decadal (15-year) Gaussian kernel to remove long-term trends. For the monthly time series, the Gaussian kernel is applied separately to each calendar month to isolate the trend and interannual variability within each month. Next, we normalize the data by removing the mean seasonal cycle and dividing by the seasonal

standard deviations, which helps satisfy the stationarity assumption and reduce false positive detection rates (Krich et al., 2020). Finally, we mask the data to include only samples from the peak melting season (June to August; JJA) at time t, whereas at times $t - n$ ($1 \leq n \leq \tau_{\max}$) samples can also come from outside the mask.

2.4. Experiment Design

Establishing reliable causation in complex climate systems requires a robust study design. First, we compare causal graphs from CESM2 and the RCMs over the historical period 1975–2014, using monthly mean outputs. Although the SEB equation describes local, instantaneous melt contributions operating within the diurnal cycle, our analysis focuses on monthly anomalies and GrIS-scale averages, where other processes (such as atmospheric variability, atmosphere-surface feedbacks, and spatial heterogeneity) become important and thus can modify the causal relationships between SEB fluxes and melt. For LENS2, we construct a summary causal graph by selecting the most frequent link type for each variable pair, with link color representing the averaged cross-MCI of this link type and link width proportional to its frequency across ensemble members. Similarly, the average auto-MCI is plotted for each node only if the majority of members have significant auto-MCI. For the RCMs, we use a bootstrap method with 100 realizations and define the link width based on the detection rate. We also examine daily RCM causal graphs to assess how causal relationships differ at higher temporal resolution. With enough sampling at daily frequency, to increase robustness, we apply PCMCI$^+$ to four consecutive 10-year periods (1975–1984, 1985–1994, 1995–2004, and 2005–2014) and then summarize a causal graph with the most frequent link types. Next, to investigate the impact of global warming on the causal relationships, we apply PCMCI$^+$ to 2061–2100 simulations from LENS2 under the SSP3-7.0 scenario and compare the resulting causal graph with the historical (1975–2014) graph.

3. Results

3.1. Evaluation of Melt Causality in CESM2

During the historical period, the CESM2 LENS2 causal graph agrees with RACMO and MAR in identifying contemporaneous positive links from melt to net shortwave radiation $(Melt \rightarrow SW_n)$ and from sensible heat flux to melt ($SH \rightarrow Melt$), and agrees with MAR in additionally detecting a contemporaneous positive link from latent heat flux to melt ($LH \rightarrow Melt$) (Figures 1a–1c). These align with the strongest lag-0 correlations in the lagged correlation analysis (Figures 2b, 2d, and 2e). Physically, the melt–shortwave relationship is expected to be bidirectional due to the melt–albedo feedback. However, PCMCI$^+$ enforces acyclicity, so contemporaneous feedback loops cannot appear; the detected direction likely reflects the dominant influence of melt-induced albedo reduction on absorbed shortwave radiation. The links $SH \rightarrow Melt$ and $LH \rightarrow Melt$ highlight the consistent effect of turbulent heating, which can be amplified during warm air intrusion and high-wind events. Unlike the RCM graphs, significant auto-MCI of *Melt* is detected in LENS2 (Figure 1c), indicating that melt persistence contributes to melt anomalies. However, this link becomes insignificant under a more conservative significance threshold (Figure S1 in Supporting Information S1), suggesting limited robustness. A similar sensitivity to the significance level is found for RACMO (Figure S1 in Supporting Information S1).

Despite agreement in link detection, link strengths (cross-MCI) differ across models. The link $SH \rightarrow Melt$ consistently exhibits the largest (or near-largest) strength (0.67, 0.68, and 0.56 for RACMO, MAR, and LENS2, respectively; Table S1 in Supporting Information S1), suggesting that *SH* exerts a strong and consistent impact on monthly melt anomalies. In RACMO, $Melt \rightarrow SW_n$ has a strength (0.63) comparable to $SH \rightarrow Melt$, whereas in MAR the other significant links are weaker (0.45 for $Melt \rightarrow SW_n$ and 0.41 for $LH \rightarrow Melt$). In LENS2, $LH \rightarrow Melt$ is comparable in strength (0.60) to $SH \rightarrow Melt$, indicating a relatively stronger role of latent heat flux, potentially related to smoother model topography in CESM2 that facilitates more moisture intrusions onto the ice sheet. By contrast, the strengths of $Melt \rightarrow SW_n$ and the auto-MCI of *Melt* are lower (0.39 and 0.25, respectively).

Overall, the results consistently identify *SH* and SW_n as primary drivers of summer surface melt anomalies on monthly timescales across models, with *LH* as an additional driver except for RACMO. The results also reveal model-dependent differences in the relative importance of these drivers, likely reflecting structural and parameterization differences. For example, the RCMs prescribe bare ice albedo using updated observational data sets (Fettweis et al., 2020; Noël et al., 2018), which may contribute to differences in the strength of the $Melt \rightarrow SW_n$ link.

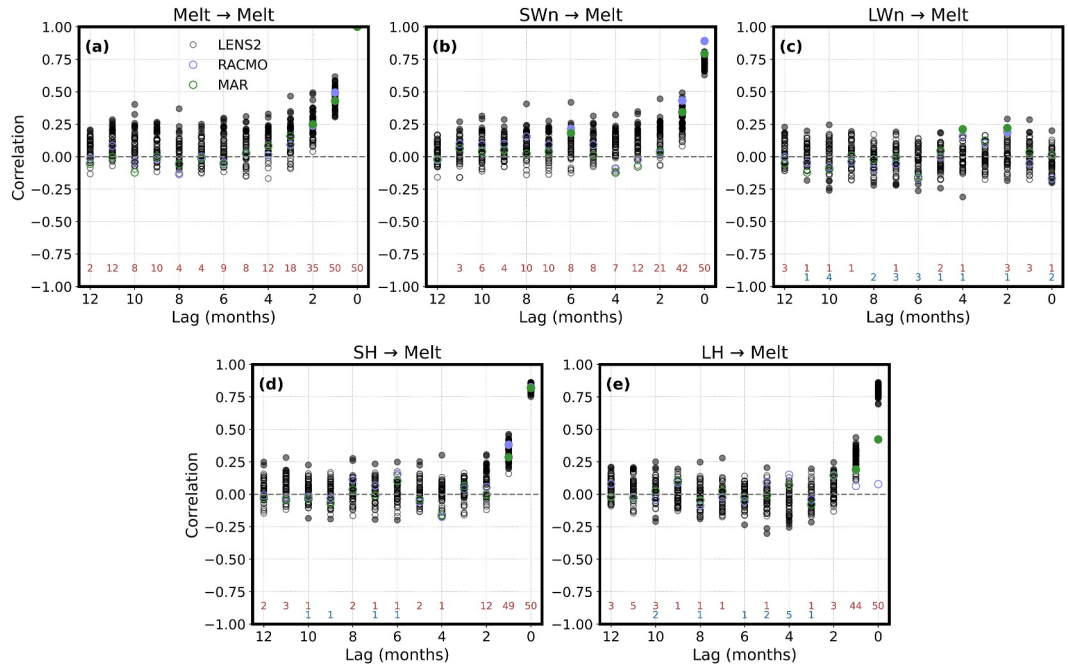

Figure 2. Lagged correlation between each variable with *Melt* during 1975–2014: (a) *Melt*, (b) SW_n, (c) LW_n, (d) *SH*, and (e) *LH*. The lagged correlations are calculated between each variable within a 3-month moving window and JJA surface melt using the monthly time series. For each lag, all individual months within the corresponding window are concatenated (e.g., May–July for a 1-month lag). Filled circles represent significant correlations at a significance level of 0.05 (95% confidence). The red (blue) numbers at the bottom indicate the number of LENS2 members that have significant positive (negative) correlations at each lag.

RACMO does not exhibit a positive contemporaneous *LH* → *Melt* link as in MAR and LENS2 across all tested significance levels (Figure S1 in Supporting Information S1), consistent with its near-zero and insignificant lag-0 correlation (Figure 2e). This difference may partly reflect internal variability, given that only one RACMO simulation is available, but could also arise from differences in the representation and variability of turbulent heat fluxes. Further investigation using controlled sensitivity experiments or process-oriented diagnostics within a consistent modeling framework would be needed to isolate the mechanisms underlying this discrepancy.

No model detects causal links between LW_n and *Melt*, despite known contributions of longwave forcing during cloudy or warm events. Due to the algorithmic construction of PCMCI$^+$, the absence of links is a more robust result than their presence (Runge, Nowack, et al., 2019). During melt, surface temperature is constrained near the melting point, limiting variability in upward longwave radiation. Although downward longwave radiation varies with atmospheric conditions, its monthly anomalies largely covary with shortwave and turbulent fluxes, providing limited independent predictive power. Compensating changes in shortwave radiation may further reduce its net effect on melt.

We observe that the causal graphs vary considerably across LENS2 ensemble members (Figure S2 in Supporting Information S1), reflecting internal variability and potential methodological limitations. On the one hand, it reflects the chaotic nature of the climate system, whereby small differences in initial conditions give rise to different relative importance of energy balance terms in driving interannual melt anomalies across realizations within the 40-year period. On the other hand, PCMCI$^+$ may struggle to consistently resolve causal dependencies in surface melt processes at monthly resolution. The observed degree of variation, such as inconsistent directions or additional links across realizations, suggests that methodological constraints likely play a more dominant role than internal variability. Such differences were also observed in other ensemble-based causal studies (Karmouche et al., 2023). This highlights the need for careful interpretation when applying causal discovery to climate variables.

3.2. Compare to Lagged Correlation

For comparison, we also calculate lagged correlations between each energy flux (and melt) within a 3-month moving window and JJA surface melt, using the processed monthly time series (Section 2.3) during 1975–2014 (Figure 2). For each lag, all individual months within the corresponding window are concatenated (e.g., May–July for a 1-month lag). At zero lag, both RCMs and all LENS2 members show significant positive correlations between SW_n and *Melt* (Figure 2b) and between *SH* and *Melt* (Figure 2d), while MAR and all LENS2 members also show significant positive correlations between *LH* and *Melt* (Figure 2e). At a 1-month lag, SW_n and *SH* remain significantly correlated with *Melt* in both RCMs (Figures 2b and 2d) and *LH* remains significantly correlated with *Melt* in MAR (Figure 2e), with the same signs as at lag 0 but weaker correlations. In LENS2, SW_n, *SH*, and *LH* remain significantly correlated with *Melt* for most ensemble members (Figures 2b, 2d, and 2e). *Melt* itself shows strong autocorrelation at lag 1 and lag 2 in both RCMs and most LENS2 members (Figure 2a). At longer lags, occasional significant correlations are also detected in some LENS2 members and in the RCMs, but they are less consistent across models.

Compared to lagged correlation, PCMCI$^+$ identifies fewer highly relevant links, typically at shorter or zero lags. Lagged correlation is prone to spurious links and larger (correlative) lags resulting from strong autocorrelation, which can bias the analysis of time delays and the quantification of the interaction mechanism (Runge et al., 2014). In contrast, PCMCI$^+$ conditions on relevant variables and past values using independence tests, filtering out these spurious associations and yielding a more interpretable network, consistent with findings from other studies (Krich et al., 2020).

3.3. Melt Causality at Daily Timescales

Since PCMCI$^+$ rarely detects robust lagged causal relationships involving surface melt at monthly resolution (Figure 1; Figure S2 in Supporting Information S1), we additionally apply the algorithm to daily time series of the five variables from the RCMs. Unlike at monthly timescales, local and synoptic processes dominate the diurnal variability of surface melt, whereas large-scale atmospheric variability plays a more limited role (van den Broeke et al., 2023). A key difference from the monthly results is that the daily graphs exhibit large significant auto-MCI values for all variables (Figure 3), consistent with stronger self-dependency in higher-frequency climate data. The significant auto-MCI of *Melt* highlights the preconditioning effect of melt from the previous day (largest auto-MCI at lag one). In RACMO, the contemporaneous positive link between SW_n and *Melt* becomes undirected with conflicting adjacencies (Figure 3a), likely reflecting the melt-albedo feedback operating at daily resolution, with comparable influence in both directions. A positive undirected contemporaneous link *SH* $\times$–$\times$ *Melt* is detected in both models (Figure 3), likely due to bidirectional interactions at daily resolution (*SH* causes *Melt* and *Melt* can also enhance *SH* by, e.g., increasing surface roughness). Consistent with its monthly causal graph (Figure 1b), MAR also exhibits a positive contemporaneous link between *Melt* and *LH*, although the detected direction is reversed (*Melt* $\rightarrow$ *LH*), which may similarly arise from short-timescale surface-atmosphere interactions. In both models, the auto-MCI of *Melt* (RACMO: 0.46; MAR: 0.50) and the cross-MCI of *SH* $\times$–$\times$ *Melt* (RACMO: 0.59; MAR: 0.57) are of comparable magnitude (Table S1 in Supporting Information S1). In RACMO, SW_n $\times$–$\times$ *Melt* also has similar strength (0.48), whereas in MAR, the links *Melt* $\rightarrow$ SW_n and *Melt* $\rightarrow$ *LH* are substantially weaker (0.15 and 0.12, respectively).

Together, these results suggest that at daily timescales, in addition to net shortwave radiation and turbulent heat fluxes, melt persistence is another dominant contributor to surface melt anomalies, although the relative importance of these processes differs between models.

3.4. Melt Causality Change Under a Warming Scenario

By the end of the century under SSP3-7.0, contemporaneous causal links persist in LENS2, but the directions of the turbulent heat-related links vary (Figure 1d). During 2061–2100, differences among ensemble-member causal graphs are also evident (Figure S3 in Supporting Information S1), reflecting internal variability in inferred melt–energy relationships and potential methodological limitations. The most frequent link types between *SH*/*LH* and *Melt* become undirected, as the collider and orientation rules cannot be applied in most ensemble members, indicating a reduction in orientability: although *SH*/*LH* and *Melt* remain conditionally dependent, the conditional independence structure no longer provides sufficient constraints to uniquely identify a dominant direction.

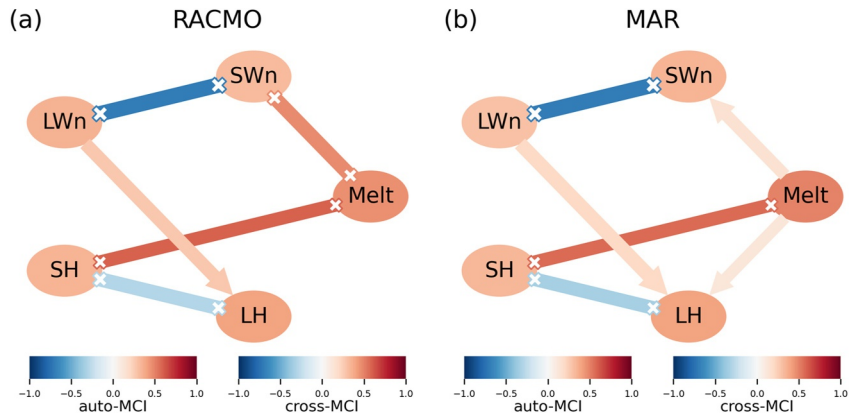

Figure 3. Causal graphs at daily frequency of the historical period 1975–2014 for RACMO (a) and MAR (b) with a significance level of 0.05. Unoriented contemporaneous links denote a conflicting adjacency when orientation rules disagree ("×–×"). Link width increases monotonically with detection rate (0%–100%), defined as the mean percentage of bootstrap realizations in which the link type is detected over the four consecutive 10-year periods from 1975 to 2014. Other causal graph conventions are the same as in Figure 1.

Several factors may contribute to this reduced orientability. First, under late-century warming, the surface across much of the ablation zone more frequently reaches and remains near the melting point from late spring through summer (Figures S4d–S4f in Supporting Information S1), potentially shortening the response time of melt to turbulent heat flux anomalies and rendering the causal direction statistically indistinguishable. Second, stronger co-variability among SEB components under warmer and moister atmospheric conditions (Table S2 in Supporting Information S1) may increase redundancy among predictors, thereby reducing the asymmetry in conditional dependencies required for orientation. Third, the turbulent flux–melt relationship is inherently nonlinear and regime-dependent. Under sustained late-century melt conditions, the effective sensitivity of melt to additional flux anomalies may change. Such regime shifts can alter the conditional dependence structure captured by linear partial-correlation tests, reducing orientability even if the underlying physical direction remains unchanged.

Therefore, the undirected $SH \circ\!\!-\!\!\circ Melt$ and $LH \circ\!\!-\!\!\circ Melt$ links likely reflect stronger and more synchronous surface-atmosphere coupling, but may also arise from reduced statistical identifiability due to increased simultaneity, shared variability, or regime-dependent sensitivity. These results should thus be interpreted as a transition toward more tightly coupled yet less statistically distinguishable interactions, rather than a definitive shift in physical causal direction.

4. Discussion and Conclusions

This study explores the potential of the PCMCI$^+$ causal discovery method to disentangle interactions between GrIS surface melt and surface energy fluxes. Compared with correlations, PCMCI$^+$ identifies fewer but more interpretable dependencies. During 1975–2014, causal graphs from CESM2 LENS2 and the higher-resolution RCMs (RACMO and MAR) consistently reveal contemporaneous positive links from melt to net shortwave radiation $(Melt \rightarrow SW_n)$ and from sensible heat flux to melt $(SH \rightarrow Melt)$, highlighting shortwave radiation and sensible heating as dominant drivers of ablation-zone summer melt anomalies. LENS2 and MAR also show a positive link from latent heat flux to melt $(LH \rightarrow Melt)$, suggesting that latent heat exchange may further contribute to melt variability in these models. Since PCMCI$^+$ enforces acyclicity, the bidirectional melt–shortwave feedback appears as a single detected link $(Melt \rightarrow SW_n)$. Although link detection is broadly consistent, link strengths vary across models, reflecting differences in the relative importance of processes. By the end of the century under SSP3-7.0, these contemporaneous positive links persist, but the turbulent heat-related links become undirected, indicating stronger atmosphere-surface coupling and/or reduced statistical identifiability in a warmer climate.

A key challenge of causal discovery in Earth science is the lack of ground truth for verifying causal graphs. Long-term, GrIS-wide surface melt observations were unavailable at the time of this study (Zheng et al., 2022). A new passive microwave-derived data set extending the record to 31 years has recently been released (Zheng

et al., 2025). A preliminary PCMCI$^+$ test combining its GrIS-integrated melt product with ablation zone-averaged SEB fluxes from ERA5 reanalysis (Hersbach et al., 2020) detected only significant melt auto-dependence and no robust SEB–melt links (not shown). This outcome likely reflects inconsistencies arising from independent retrieval algorithms and associated uncertainties across the different data sources, which can obscure cross-variable dependencies in a causal framework. Integrating observational data into causal frameworks remains an important future direction. Model-based inference introduces additional uncertainty. Although the RCMs and CESM2 simulate reasonable GrIS SEB and surface melt (Fettweis et al., 2017; Noël et al., 2018; van Kampenhout et al., 2020), the prominence and orientation of inferred causal links depend on model representations of surface processes and snow/ice properties, and are therefore subject to structural biases (Holube et al., 2022). In particular, CESM2 biases associated with relatively coarse horizontal resolution, such as cloud-driven radiation variability, wind and near-surface gradients controlling turbulent flux variability, and surface-state persistence (e.g., albedo and snow wetness) may influence the detected causal links (Herrington et al., 2022; van Kampenhout et al., 2019; Yin et al., 2025). These considerations suggest that projected future changes are best interpreted as CESM2-conditional hypotheses, motivating future multi-model tests. Nonetheless, causal analysis of state-of-the-art models provides valuable insight into process representation and future evolution (Galytska et al., 2023; Karmouche et al., 2023; Nowack et al., 2020). The agreement of key links across models increases confidence in the main findings.

Robustness was assessed by varying significance level (0.025, 0.05, and 0.1; Figures S1 and S5 in Supporting Information S1), maximum lag (6- to 18-month; 5- to 25-day; not shown), and analysis length (30–50 years; not shown). The melt-related links persist under these variations, though directions occasionally change. We also evaluate the impact of differing ablation masking in different models and time periods at monthly timescales by applying the RACMO 1975–2014 mean ablation mask (remapped to the MAR and CESM2 grids; Figure S6 in Supporting Information S1). The resulting graphs remain largely unchanged, except that the *Melt* auto-MCI in LENS2 becomes insignificant during 1975–2014. This suggests that differences in ablation masking exert only a minor influence on the inferred melt-related links.

We note that our findings primarily apply to the GrIS ablation zone and do not necessarily extend to higher-elevation percolation regions. Compared to the LENS2 ablation-zone graphs (Figures 1c and 1d), no significant contemporaneous link between SW_n and *Melt* is detected either over the period-specific percolation zones or over the fixed elevation band between 1 and 2 km, while the other significant melt-related links remain broadly similar (Figures S7 and S8 in Supporting Information S1). These results suggest that the melt–shortwave radiation relationship identified over the ablation zone is substantially weaker at higher elevations, likely because large areas within the percolation zone continue to experience relatively limited surface albedo anomaly variability even under SSP3-7.0 warming. In contrast, turbulent heat flux links remain robust across regions, highlighting their important role in higher-elevation melt anomaly variability in CESM2.

Limitations remain in applying causal discovery to ice sheet surface melt processes. Causal discovery requires more sophisticated assumptions. For example, PCMCI$^+$ assumes causal sufficiency, requiring that all relevant variables be included. Although focusing on melt-related links mitigates this issue, omitted variables—such as near-surface air temperature or cloud properties—may still influence results. Nonlinear relationships are also possible. Given the relatively short 40-year segments analyzed here, linear conditional independence tests provide a reasonable approximation and have been shown to offer stronger detection power and interpretability when linearity dominates (Krich et al., 2020; Runge, Nowack, et al., 2019). Temporal resolution presents another challenge. At daily or higher frequencies, GrIS-wide surface melt data from observations or models are limited. Single AWS-based surface melt calculated from measured energy fluxes contains frequent missing data and intermittent zero-melt periods due to temperature fluctuations around 0°C. Such threshold-controlled variability challenges the PCMCI$^+$ framework applied here, which uses the linear RobustParCorr conditional independence test. Furthermore, constructing sufficiently long and continuous AWS records would require reliable gap-filling approaches, whose influence on PCMCI + causal graphs remains unclear. Daily-scale experiments with the RCMs indicate strong one-day melt self-dependence, while other significant links remain contemporaneous and often undirected. Finally, determining the direction of contemporaneous links remains challenging, and inferred directions should be interpreted with appropriate caution. Future work could explore alternative causal discovery methods (Ali et al., 2024; Docquier et al., 2024), incorporate additional data sets (Zheng et al., 2025), investigate

specific atmospheric process chains (Kromer & Trusel, 2023), compare across regions, and conduct targeted sensitivity experiments.

Understanding the evolving coupling between GrIS surface melt variability and climate is critical, as this relationship will increasingly control future melt-dominated SMB variability and influence ice dynamics, freshwater fluxes, ocean circulation, and sea level rise (Fyke et al., 2014; Hanna et al., 2024). Our results demonstrate the feasibility of applying causal discovery to simulated climate data while highlighting several challenges—such as variable completeness, temporal resolution, and contemporaneous orientation—that must be addressed, underscoring the need for further methodological development in ice sheet-atmosphere studies.

Conflict of Interest

The authors declare no conflicts of interest relevant to this study.

Availability Statement

CESM2 is an open-source model, available via the CESM GitHub repository (https://github.com/ESCOMP/CESM). The CESM2 LENS2 (CMIP6) ensemble simulations used in this study are publicly available at Danabasoglu, Deser, et al. (2020). The code and data for generating the plots are available in an open repository on Zenodo (Yin, 2025).

Acknowledgments
ZY, ACS, RTD, SA, OF, and JW are supported by the NSF HDR iHARP institute (Grant 2118285). JW is also supported by an NSF Grant (1942714). Analyzing and data storage resources, including the Cheyenne supercomputer (Computational and Information Systems Laboratory, 2017), were provided by the Computational and Information Systems Laboratory (CISL) at NSF National Center for Atmospheric Research (NCAR), a major facility sponsored by the NSF under Cooperative Agreement 1852977. We thank Brice Noël for providing RACMO2.3p2 data (Noël et al., 2018), and Xavier Fettweis for providing MARv3.14 data (Haacker et al., 2024). We also thank Nander Wever, Nicole-Jeanne Schlegel, Yiyi Huang, and Md Osman Gani for providing other model data and for valuable discussions and comments on this work. Finally, we thank the editor Christine Dow, reviewer Luke Trusel, and the other two anonymous reviewers for their insightful comments that helped improve the manuscript.

References

Ali, S., Hasan, U., Li, X., Faruque, O., Sampath, A., Huang, Y., et al. (2024). Causality for earth science – a review on time-series and spatiotemporal causality methods. Retrieved from https://arxiv.org/abs/2404.05746

Box, J. E., Hubbard, A., Bahr, D. B., Colgan, W. T., Fettweis, X., Mankoff, K. D., et al. (2022). Greenland ice sheet climate disequilibrium and committed sea-level rise. *Nature Climate Change*, *12*(9), 808–813. https://doi.org/10.1038/s41558-022-01441-2

Computational and Information Systems Laboratory. (2017). *Cheyenne: HPE/SGI ICE XA system (Climate Simulation Laboratory)*. National Center for Atmospheric Research. https://doi.org/10.5065/D6RX99HX

Danabasoglu, G., Deser, C., Rodgers, K., & Timmermann, A. (2020). CESM2 large ensemble [Dataset]. *NSF National Center for Atmospheric Research*. https://doi.org/10.26024/kgmp-c556

Danabasoglu, G., Lamarque, J.-F., Bacmeister, J., Bailey, D. A., DuVivier, A. K., Edwards, J., et al. (2020). The community earth system model version 2 (cesm2). *Journal of Advances in Modeling Earth Systems*, *12*(2), e2019MS001916. https://doi.org/10.1029/2019MS001916

Docquier, D., Di Capua, G., Donner, R. V., Pires, C. A. L., Simon, A., & Vannitsem, S. (2024). A comparison of two causal methods in the context of climate analyses. *Nonlinear Processes in Geophysics*, *31*(1), 115–136. https://doi.org/10.5194/npg-31-115-2024

Du, D., Subramanian, A. C., Han, W., Ninad, U., & Runge, J. (2024). Causal analysis discovers an enhanced impact of tropical western Pacific on Indian summer monsoon subseasonal anomalies. *Geophysical Research Letters*, *51*(10), e2023GL106431. https://doi.org/10.1029/2023GL106431

Fausto, R. S., van As, D., Box, J. E., Colgan, W., Langen, P. L., & Mottram, R. H. (2016). The implication of nonradiative energy fluxes dominating Greenland ice sheet exceptional ablation area surface melt in 2012. *Geophysical Research Letters*, *43*(6), 2649–2658. https://doi.org/10.1002/2016GL067720

Fettweis, X., Box, J. E., Agosta, C., Amory, C., Kittel, C., Lang, C., et al. (2017). Reconstructions of the 1900–2015 Greenland ice sheet surface mass balance using the regional climate mar model. *The Cryosphere*, *11*(2), 1015–1033. https://doi.org/10.5194/tc-11-1015-2017

Fettweis, X., Hofer, S., Krebs-Kanzow, U., Amory, C., Aoki, T., Berends, C. J., et al. (2020). Grsmbmip: Intercomparison of the modelled 1980–2012 surface mass balance over the Greenland ice sheet. *The Cryosphere*, *14*(11), 3935–3958. https://doi.org/10.5194/tc-14-3935-2020

Fyke, J. G., Vizcaíno, M., Lipscomb, W., & Price, S. (2014). Future climate warming increases Greenland ice sheet surface mass balance variability. *Geophysical Research Letters*, *41*(2), 470–475. https://doi.org/10.1002/2013GL058172

Galytska, E., Weigel, K., Handorf, D., Jaiser, R., Köhler, R., Runge, J., & Eyring, V. (2023). Evaluating causal arctic-midlatitude teleconnections in cmip6. *Journal of Geophysical Research: Atmospheres*, *128*(17), e2022JD037978. https://doi.org/10.1029/2022JD037978

Haacker, J., Wouters, B., Fettweis, X., Glissenaar, I. A., & Box, J. E. (2024). Atmospheric-river-induced foehn events drain glaciers on novaya zemlya. *Nature Communications*, *15*(1), 7021. https://doi.org/10.1038/s41467-024-51404-8

Hanna, E., Topál, D., Box, J. E., Buzzard, S., Christie, F. D., Hvidberg, C., et al. (2024). Short-and long-term variability of the antarctic and Greenland ice sheets. *Nature Reviews Earth & Environment*, *5*(3), 193–210. https://doi.org/10.1038/s43017-023-00509-7

Herrington, A. R., Lauritzen, P. H., Lofverstrom, M., Lipscomb, W. H., Gettelman, A., & Taylor, M. A. (2022). Impact of grids and dynamical cores in cesm2.2 on the surface mass balance of the Greenland ice sheet. *Journal of Advances in Modeling Earth Systems*, *14*(11), e2022MS003192. https://doi.org/10.1029/2022MS003192

Hersbach, H., Bell, B., Berrisford, P., Hirahara, S., Horányi, A., Muñoz-Sabater, J., et al. (2020). The era5 global reanalysis. *Quarterly Journal of the Royal Meteorological Society*, *146*(730), 1999–2049. https://doi.org/10.1002/qj.3803

Holube, K. M., Zolles, T., & Born, A. (2022). Sources of uncertainty in Greenland surface mass balance in the 21st century. *The Cryosphere*, *16*(1), 315–331. https://doi.org/10.5194/tc-16-315-2022

Karmouche, S., Galytska, E., Runge, J., Meehl, G. A., Phillips, A. S., Weigel, K., & Eyring, V. (2023). Regime-oriented causal model evaluation of Atlantic–Pacific teleconnections in cmip6. *Earth System Dynamics*, *14*(2), 309–344. https://doi.org/10.5194/esd-14-309-2023

Krich, C., Runge, J., Miralles, D. G., Migliavacca, M., Perez-Priego, O., El-Madany, T., et al. (2020). Estimating causal networks in biosphere–atmosphere interaction with the pcmci approach. *Biogeosciences*, *17*(4), 1033–1061. https://doi.org/10.5194/bg-17-1033-2020

Kromer, J. D., & Trusel, L. D. (2023). Identifying the impacts of sea ice variability on the climate and surface mass balance of West Antarctica. *Geophysical Research Letters*, *50*(18), e2023GL104436. https://doi.org/10.1029/2023GL104436

Mattingly, K. S., Turton, J. V., Wille, J. D., Noël, B., Fettweis, X., Rennermalm, Å. K., & Mote, T. L. (2023). Increasing extreme melt in northeast Greenland linked to foehn winds and atmospheric rivers. *Nature Communications*, *14*(1), 1743. https://doi.org/10.1038/s41467-023-37434-8

Noël, B., van de Berg, W. J., van Wessem, J. M., van Meijgaard, E., van As, D., Lenaerts, J. T. M., et al. (2018). Modelling the climate and surface mass balance of polar ice sheets using racmo2 – Part 1: Greenland (1958–2016). *The Cryosphere*, *12*(3), 811–831. https://doi.org/10.5194/tc-12-811-2018

Nowack, P., Runge, J., Eyring, V., & Haigh, J. D. (2020). Causal networks for climate model evaluation and constrained projections. *Nature Communications*, *11*(1), 1415. https://doi.org/10.1038/s41467-020-15195-y

Rodgers, K. B., Lee, S.-S., Rosenbloom, N., Timmermann, A., Danabasoglu, G., Deser, C., et al. (2021). Ubiquity of human-induced changes in climate variability. *Earth System Dynamics*, *12*(4), 1393–1411. https://doi.org/10.5194/esd-12-1393-2021

Runge, J. (2020). Discovering contemporaneous and lagged causal relations in autocorrelated nonlinear time series datasets. In *Conference on uncertainty in artificial intelligence* (pp. 1388–1397).

Runge, J., Bathiany, S., Bollt, E., Camps-Valls, G., Coumou, D., Deyle, E., et al. (2019). Inferring causation from time series in earth system sciences. *Nature Communications*, *10*(1), 2553. https://doi.org/10.1038/s41467-019-10105-3

Runge, J., Gerhardus, A., Varando, G., Eyring, V., & Camps-Valls, G. (2023). Causal inference for time series. *Nature Reviews Earth & Environment*, *4*(7), 487–505. https://doi.org/10.1038/s43017-023-00431-y

Runge, J., Nowack, P., Kretschmer, M., Flaxman, S., & Sejdinovic, D. (2019). Detecting and quantifying causal associations in large nonlinear time series data sets. *Science Advances*, *5*(11), eaau4996. https://doi.org/10.1126/sciadv.aau4996

Runge, J., Petoukhov, V., & Kurths, J. (2014). Quantifying the strength and delay of climatic interactions: The ambiguities of cross correlation and a novel measure based on graphical models. *Journal of Climate*, *27*(2), 720–739. https://doi.org/10.1175/JCLI-D-13-00159.1

Samarasinghe, S. M., McGraw, M. C., Barnes, E. A., & Ebert-Uphoff, I. (2019). A study of links between the arctic and the midlatitude jet stream using granger and pearl causality. *Environmetrics*, *30*(4), e2540. https://doi.org/10.1002/env.2540

Slater, T., Shepherd, A., McMillan, M., Leeson, A., Gilbert, L., Muir, A., et al. (2021). Increased variability in Greenland ice sheet runoff from satellite observations. *Nature Communications*, *12*(1), 6069. https://doi.org/10.1038/s41467-021-26229-4

van den Broeke, M. R., Kuipers Munneke, P., Noël, B., Reijmer, C., Smeets, P., van de Berg, W. J., & van Wessem, J. M. (2023). Contrasting current and future surface melt rates on the ice sheets of Greenland and Antarctica: Lessons from in situ observations and climate models. *PLOS Climate*, *2*(5), 1–17. https://doi.org/10.1371/journal.pclm.0000203

van den Broeke, M. R., Smeets, C. J. P. P., & van de Wal, R. S. W. (2011). The seasonal cycle and interannual variability of surface energy balance and melt in the ablation zone of the west Greenland ice sheet. *The Cryosphere*, *5*(2), 377–390. https://doi.org/10.5194/tc-5-377-2011

van Kampenhout, L., Lenaerts, J. T. M., Lipscomb, W. H., Lhermitte, S., Noël, B., Vizcaíno, M., et al. (2020). Present-day Greenland ice sheet climate and surface mass balance in cesm2. *Journal of Geophysical Research: Earth Surface*, *125*(2), e2019JF005318. https://doi.org/10.1029/2019JF005318

van Kampenhout, L., Rhoades, A. M., Herrington, A. R., Zarzycki, C. M., Lenaerts, J. T. M., Sacks, W. J., & van den Broeke, M. R. (2019). Regional grid refinement in an earth system model: Impacts on the simulated Greenland surface mass balance. *The Cryosphere*, *13*(6), 1547–1564. https://doi.org/10.5194/tc-13-1547-2019

Vannitsem, S., Dalaiden, Q., & Goosse, H. (2019). Testing for dynamical dependence: Application to the surface mass balance over Antarctica. *Geophysical Research Letters*, *46*(21), 12125–12135. https://doi.org/10.1029/2019GL084329

Wang, W., Zender, C. S., van As, D., Fausto, R. S., & Laffin, M. K. (2021). Greenland surface melt dominated by solar and sensible heating. *Geophysical Research Letters*, *48*(7), e2020GL090653. https://doi.org/10.1029/2020GL090653

Yin, Z. (2025). IceZYin/2023-GrIS-melt-causality [Collection]. *Zenodo*. https://doi.org/10.5281/zenodo.16541778

Yin, Z., Herrington, A. R., Datta, R. T., Subramanian, A. C., Lenaerts, J. T. M., & Gettelman, A. (2025). Improved understanding of multicentury Greenland ice sheet response to strong warming in the coupled cesm2-cism2 with regional grid refinement. *Journal of Advances in Modeling Earth Systems*, *17*(2), e2024MS004310. https://doi.org/10.1029/2024MS004310

Zheng, L., Cheng, X., Shang, X., Chen, Z., Liang, Q., & Wang, K. (2022). Greenland ice sheet daily surface melt flux observed from space. *Geophysical Research Letters*, *49*(6), e2021GL096690. https://doi.org/10.1029/2021GL096690

Zheng, L., Shang, X., Van Den Broeke, M. R., Noël, B., Li, X., Fettweis, X., et al. (2025). Rapid increases in satellite-observed ice sheet surface meltwater production. *Nature Climate Change*, *15*(7), 769–774. https://doi.org/10.1038/s41558-025-02364-4